Development of a novel high temperature open tribometer with laser-based heating system

T. Leveille, D. Fabre, Mehmet Cici, Julien Sijobert, M. Doubenskaia, C. Courbon

Development of a novel high temperature open tribometer with laser-based heating system

T. Leveille[a], D. Fabre[a], M. Cici[a], J. Sijobert[a], M. Doubenskaia[a], C. Courbon[a,*]

[a] *University of Lyon, CentraleLyon-ENISE, CNRS, LTDS UMR 5513, F-42023, Saint-Etienne, France*

Abstract

Contacts operating under severe conditions such as high temperatures, contact pressures and/or sliding velocities, can occur in many applications and especially in metalworking processes. The extreme thermomechanical loadings withstood by the tooling during such interaction directly govern their lifetime but also the functional properties of the component surface. Understanding the friction and wear mechanisms behind is still an issue and can only be addressed with a relevant experimental set-up. This work presents the development of a new laser-based heating system fitted on an open tribometer with the aim of investigating such severe contact conditions for a AISI1045 carbon steel during sliding against uncoated cemented carbide. A 3D numerical approach is adopted to design the system and predict the temperature distribution, as well as the heating rates, below the laser beam and at the expected contact zone. A phase transformation model based on the simulated thermal kinetics is applied to identify the conditions leading to the potential formation of austenite and to show that a proper combination of laser power and sliding velocity has to be selected to ensure the desired contact conditions. It is shown for example that even at high sliding velocities, a maximum temperature of 600°C can be reached in the contact zone without exceeding the melting temperature ahead while only a thin layer can be affected by the laser. The experimental set-up is described with the integration of a laser head into the test bench. An experimental campaign is carried out to show the influence of the temperature and sliding conditions on the tribological behavior especially in terms of friction, wear mechanisms and microstructural evolution beneath the contact track.

Keywords: High temperature, Friction, Laser preheating, Microstructural evolution

*Corresponding Author. Tel.: +33 4 77 43 75 58
Email address: cedric.courbon@enise.fr (C. Courbon)

1. Introduction

Over the last decades, an increasing demand for solutions to enhance the tribological behavior of mechanical systems regards to the temperature has been observed. This is often the result of the increasing requirements in terms of performance and durability, pushing them to operate under much more severe conditions. Whether directly via the operating environment or indirectly due to the sliding conditions [1], numerous applications are concerned by elevated temperature issues in several key industries, such as aerospace (turbo-engines), automobile (combustion engines or braking systems), power generation (gas turbines) but also in many metalworking processes (hot rolling, hot forming or machining). Despite the growing effort in the field of high temperature tribology, a clear understanding on how the temperature affects the wear and frictional behavior is still needed to improve their efficiency, functionality or lifetime. Being able to run experimental campaigns simulating the contact conditions in these various applications appears crucial to reach this objective.

In the literature, several research groups endeavored to develop dedicated set-ups to investigate contacts occurring at elevated temperature.

The first conventional option is to heat the working environment and fit a tribometer into a heating chamber. Mane et al. [2] designed their own ball-on-ring tribometer within a furnace to study the effect of temperature up to 60°C on the wear of reinforced rubber materials for tire industry. Tran et al. [3] selected a commercial UMT pin-on-disc with a heating furnace and performed experiments up to 700°C to study the oxide formation between a High Speed Steel and a Stainless Steel 316. A similar configuration was employed by Ghiotti et al. [4] up to 800°C on a high strength steel where the authors especially tried to simulate the thermal cycles to which the forming dies are subjected in hot stamping by periodically cooling the friction pin with an air nozzle. Rahman et al. [5] studied the Inconel 617 and alloy 800HT under high temperatures with a specially developed closed-tribometer. The latter is placed in a transparent chamber heated with infrared radiation reflected by a thin gold coated quartz tube and controlled environment to assess the impact of oxidation on the friction performance. Some other works also report the use of a hot air blower to warm up a pin-on-disc setup within the heating chamber 400°C [6].

Increasing the temperature can be achieved by heating the contact bodies themselves. Hoić et al. [7] designed a tribometer with an electric heater built in the rotary disc which allowed them to reach 250°C when testing clutch and drive train contact components.In the same way, Tavasci et al. [8] selected a ring-on-ring tribometer with heaters in the two discs to evaluate a heat transfer coefficient with a 0.40% carbon steel up to 800°C. Reciprocating contact configurations are also mostly investigated with this method. Samples are commonly heated via heating elements embedded within the sample holders such as in the work of Courbon et al. [9] focusing on adhesion tendency up to 800°C using a commercial Optimol SRV. Similarly, Velkavrh

et al. [10] employed the latter to handle temperatures up to 200°C and to characterize the tribological behaviour at high contact pressure and high velocities in bulk metal forming. Both bodies in contact can even be heated up as proposed byMary et al. [11] in blade/disk fretting wear tests up to 500°C. Alternatively to electric elements, a ball-on-disc heated by an induction system up to 800 °C was also developed by Gautam et al. [12] to study the effects of self-lubricating coatings.

Interestingly, these selected works show that the term high temperature tribology can be discussed as it highly depends on the tribological system and materials in contact. As emphasized by Meng et al. [13], a temperature considered as high for a polymeric material will indeed not be that high for a metallic material such as steel. Moreover, one can see that various technological solutions were implemented to heat the specimens and control the temperature. However, in all the cited studies, a closed-tribometer was employed. If this might be relevant for some contact configurations where wear debris recirculation, surface hardening or oxidation occur, it could be detrimental to investigate some other applications as early highlighted by Olsson et al. [14] or recently by Sterle et al. [15]. Indeed, this kind of tribometer does not provide a special contact configuration where the material is only once in contact with the counter-surface as it is in some processes like sheet forming, machining and friction stir welding.

Olsson et al. [16] proposed one of the first open bar-on-cylinder tribometer to tackle this issue. Claudin et al. [17] or BenAbdelali et al. [18] extended this concept to a pin-on-bar configuration targeting high contact pressures and sliding velocities whereas some other research groups oriented their work towards a linear scratch-test type of contact [19, 20]. In each of these set-ups, the temperature is unfortunately not controlled but is the result of the frictional heat. The largest developments in terms of open high temperature tribometers can be found in the hot forming community. Simulative tests based on strip drawing configuration were developed by Yanagida et al. [21] or Boher et al. [22] respectively using a pre-heating furnace or a resistance heating system both up to 875°C. Mozgovoy et al. [23] upgraded it and designed an innovative hot strip tribometer in which the sheet strip is mounted vertically in order to minimize the accumulation of wear debris. Heating is provided directly via the clamping jaws and the Joule effect which enables a faster heating compared to most of the high temperature set-ups with heating rates up to $35°C/s$ and temperature close to 900°C. The maximum sliding velocity that can be achieved remains limited to $0.5m/s$.

This brief literature survey shows that developing a versatile open tribometer, able to cover a wide range of contact conditions and control the operating temperature is still a real challenge. With most of the mentioned heating systems, the heating and cooling rates are relatively low and do not represent the high thermal kinetics as high as $10^5°C/s$ that can be encountered in some high temperature applications. Moreover, the use of a furnace/heating chamber can lead to the formation of thicker oxide layers and/or

undesired contamination which could adversely affect the analysis of the results. Finally, it appears that no system, to the best of the author's knowledge, is able to run high temperature controlled wear test at a high sliding velocity exceeding $2m/s$.

The proposed paper has thus a twofold objective: (i) to present the design and assess a novel approach to elevated temperature wear testing, based on a laser pre-heating system, able to cover a wide range of contact conditions especially at high sliding velocities; and (ii) to implement the concept on an existing open tribometer and give a first insight of the resulting tribological behaviour with a preliminary experimental campaign on a AISI1045 steel. The paper is organized into three main parts: the first describes the testing configuration and the modeling approach that has been developed to assess the capability of the heating system; the second part will present the numerical results in terms of achievable testing temperatures but also expected phase transformation as far as a carbon steel is concerned; the third part will introduce the integration of the heating system onto the tribometer and the results of a preliminary experimental campaign under various heat inputs and sliding conditions.

2. Design and Modeling approach

2.1. Brief description of the test configuration

An in-house made open tribometer [17, 18] was used in this study which consists in a specific device mounted in a NC lathe and developed to carry out frictional tests under high contact pressures and sliding velocities (Fig. 1a). The tribological behaviour under such conditions is investigated by scratching a pin with a spherical tip against a cylindrical bar made of the investigated material along a helicoid path.

Once the whole surface of the bar has been used, a cutting tool refreshes the surface ploughed by the pin to remove the affected layer of work material. A belt finishing operation is then applied leading to a controlled and repeatable surface roughness of Ra 0.5μm with a negative skewness Rsk (Fig. 1a).

The normal load is applied by a hydraulic jack (Fig. 1b). Friction pins are maintained by an instrumented pin-holder (Fig. 1c) fixed onto a dynamometer in order to provide the macroscopic force components.

The concept of this work was thus to upgrade this tribometer with the ability to control the input temperature of the counter surface into the contact. To this end, the idea was to implement a processing optics typically used for heat treatment onto the existing setup. The Figure 2 presents the developed configuration with the laser beam impacting the input surface.

Due to several design constraints related to the tribometer or the machine itself, the perpendicularity of the laser beam could not be achieved resulting in an incident angle of 57°. This led the initial laser spot diameter of 1.2mm to be elongated in the sliding direction, finally forming an elliptical shape of 1.2x5.5mm. From the tribological point of view, an elliptical spot appeared to be even beneficial it allowed to reach a

higher temperature under the expected contact zone with a limited temperature in the laser spot. Indeed, because of a larger spot, the heat flux density is reduced so the temperature does not reach excessively high values close to the melting temperature. Moreover, as the main length of this elliptical spot is in the material flow direction, the end of the laser spot became closer to the contact zone while the counter surface exhibits a longer exposure time. It can be noted that the distance between the end of the heated area and the entrance of the contact zone remains limited to approximately 2.75mm.

2.2. Numerical model

The first step of this work was to assess the temperatures that could effectively be achieved at the contact entrance.

A 3D Arbitrary Lagrangian Eulerian (ALE) model (Fig. 3) was implemented in the Finite Element code ABAQUS and solved with an explicit integration scheme. The ALE approach provides an efficient framework to compute stationary thermal regimes within the sliding material. The problem to solve being symmetric, only half of it was considered. In this model, the workmaterial enters via the Eulerian boundary at a given velocity by the inflow surface (A'B'C'D' in Fig. 3a-b) and goes out through the Eulerian outflow surface (ABCD in Fig. 3a-b).

The workpiece is discretized using hexagonal eight-node, coupled-temperature displacement, reduced-integration elements (C3D8RT) from the ABAQUS element library (Fig. 3b).

Beneath the pre-heated region and the expected contact zone, the element size has been decreased down to 100μm (Fig. 4b). The expected contact width has typically an order of magnitude of 1mm. The contact itself between the pin and the counter-material being not modelled, a ratio of 10 elements appears consistent to extract only thermal data from such a simulation. This mesh would have to be refined if the whole tribological problem, i.e. sliding contact between the two solids, would be modelled.

A AISI1045 steel was used in this work as a reference and well characterized material. Its behavior has been taken into account through the strain, strain rate and temperature dependent Johnson-Cook flow stress model (Eq. 1). Even if this was not necessary at this step, it has been selected to deal with the complex thermo-mechanical coupling that could be introduced in further studies. Parameters of the latter have been defined thanks to the identification provided by Jaspers and Dautzenberg [24] (Table 2).

$$\sigma_{eq} = \left[A + B\left(\varepsilon_p\right)^n\right]\left[1 + C\ln\left(\frac{\dot{\varepsilon_p}}{\dot{\varepsilon}_0}\right)\right]\left[1 - \left(\frac{T - T_0}{T_f - T_0}\right)^m\right] \tag{1}$$

where A is the yield strength (MPa), B is the hardening modulus (MPa), C is the strain rate sensitivity coefficient (viscosity), n is the hardening coefficient, m is the thermal softening coefficient, $\dot{\varepsilon}_p$ is the plastic strain rate (s^{-1}), $\dot{\varepsilon}_0$ is the reference plastic strain rate (s^{-1}) ($\dot{\varepsilon}_0 = 1s^{-1}$), T_f is the melting temperature of the work material (°C), T is the temperature of the workpiece (°C), and T_0 is room temperature (°C).

2.3. Thermal loading and boundary conditions

In the present work, the interaction between the pin and the counter-material has not been modeled as the objective was to only assess the input temperature within the contact zone. To this end, the laser beam was modeled by a heat flux density homogeneously applied over a surface similar to the laser spot and ahead of the expected contact zone as shown in Figures. 3d-e.The amplitudes of the heat flux were selected to cover a large range of power inputs. This implies that they represent the power that should be theoretically absorbed by the heated surface. To achieve this power input, absorption as well as laser performance and beam orientation should be considered and the actual power of the laser should be selected accordingly.

Additional thermal boundary conditions were applied as follows:

- Heat is dissipated by conduction through surfaces AA'D'D, ABCD, A'B'C'D' and C'CDC',
- Heat exchange by convection with the surrounding environment on the surface ABB'A' is neglected,
- Heat exchange by radiation is also neglected considering the small size of the heated regions, surface thermal gradients compared to the bulk temperatures as well as the amplitude of the investigated power inputs.

In order to implement the most reliable physics, temperature dependent thermal properties of the AISI 1045 steel were implemented as described in the Table 3.

3. Temperature predictions

3.1. Temperature distributions & kinetics

The numerical model was first employed to extract the temperature profiles at the top surface, along the edge AA' shown in Figures 3a-c. Four input powers ranging from 500 to 2000W combined to four sliding velocities of 25, 50, 75 and 100m/min were investigated.

As it can be seen on the Figure 5a, the higher the laser power the higher temperature will be at the top surface for a given sliding velocity. Temperatures up to 1200°C can be reached when applying 2000W but a sudden decrease can be observed once the sliding material leaves the heated region. The expected temperature at the contact zone appears to be about half the maximum temperature but still provides a relevant range from 150 to 600°C at 50m/min.

The Figure 5b shows that for a given input power of 1500W increasing the sliding velocity from 25 to 100m/min will reduce the maximum temperature at the exit of the heated region from 1300 to 600°C. However, as far as the temperature at the contact zone is concerned, temperatures between 350 and 500°C can still be expected.

This analysis was extended to the full matrix of conditions and led to the map in Figure 6 summarizing the achievable temperatures at the top surface of the contact zone. Over the whole range of sliding velocities, temperatures up to minimum 450°C can always be reached, even at the highest sliding velocity of 100m/min. For the latter, reaching highest temperatures would require a higher power input and thus the use of a more powerful laser source.

Temperatures exceeding 800°C within the pre-heated region were highlighted in the Figures 5a-b. This definitely raised the question of a potential phase transformation when materials such as carbon steels in this study are investigated. Temperature profiles were thus extracted along the depth, right in the axis of laser spot (Fig. 7).

It was shown that the temperature rapidly decreases along the depth, being approximately half of the top surface one at 0.2mm. Under several combinations of sliding velocity and input power, the Ac1 temperature can even be exceeded over the first 50μm. However, it can be noted that extremely fast thermal kinetics were achieved (Fig. 5) with heating rates as high as 5.10^5 $°C/s$ and cooling rates approximating 3.10^5 $°C/s$. A phase transformation model had to be developed to confirm its occurrence based on this data.

3.2. Occurrence of a phase transformation

Based on the previous findings, the question of a potential evolution in the microstructure was raised. The AISI1045 is a ferritic-pearlitic steel which, because of continuous heating, can transform into austenite. To study this phenomena and assess if this transformation could occur, a metallurgical model developed by Miokovic et al. [25, 26] and based on the Avrami equation [27] was used. The Avrami model was initially developed for isothermal transformations but in the case of high heating rates, Mioković et al. discretized the Avrami equation in several short isothermal steps (see Eq. **??**) and summed the fraction of transformed material.

$$f_{A,i+1} = f_{A,i} + \frac{\partial f_{A,i}}{\partial t}|_{t_i^*} \times \Delta t \tag{2}$$

$$\frac{\partial f_{A,i}}{\partial t}|_{t_i^*} = n.b(T_i)^n.ln\left(\frac{1}{1-f_{A,i}}\right)^{\frac{n-1}{n}}.(1-f_{A,i}) \tag{3}$$

$$b(T) = C.exp\left(-\frac{\Delta H}{k.t}\right) \tag{4}$$

where $f_{A,i+1}$ is the percentage of austenite formed at t_i^* (%), T is the temperature ($°K$), k is the Boltzmann constant ($eV.K^{-1}$), n is the Avrami constant, C is the velocity constant (s^{-1}) and ΔH is the activation enthalpy (ferrite to austenite) (eV).

The parameters used to calculate the percentage of formed austenite are reported in the Table 4. They were identified based on stress-free dilatometry tests using heating rates up to $10000°C/s$.

The fraction of formed austenite computed from Equations 2, 3 and 4 can be seen in Fig. 8 for different constant heating rates. One can observe that when increasing the heating rate, the activation of the austenitic transformation is shifted towards higher temperatures. Indeed, whereas the transformation starts around 750°C at 10^3 $°C/s$, temperatures between 900 and 925°C have to be reached at 5.10^5 $°C/s$. Another conclusion is that, higher is the heating rate, lower is the time to produce 100% of austenite once the transformation began and temperatures higher than 1000°C are exceeded within this short time. One still has to be careful and consider only the trend as these results are extrapolated up to 5.10^5 $°C/s$ from the work of Miokovic et al. [26] that was limited to 10^4 $°C/s$.

This model was then applied to the temperature kinetics extracted from the FE model (Fig. 5). The temperature profiles were then discretized in short time steps of $10^{-4}s$ and the heating rate was computed for each one. Summing the fraction of formed austenite over theses steps, it was possible to assess the total amount of austenite formed during the whole heating cycle with varying heating rates. The Figure 9 shows the fraction of formed austenite over the whole ranges of sliding velocity and laser power input.

The parameters leading to the formation of 100% of austenite can be identified and the experiments designed according to the targeted conditions when correlated to the expected temperature map shown in Figure 6. As an example, testing where austenitic transformation has to be avoided will be limited to a maximum contact temperature of 300°C at 25m/min with a 1kW input power, 400°C at 60m/min with a 1.5kW input power and almost 500°C at 100m/min with a 2kW input power

3.3. Discussion of the numerical results

The expected temperature at the contact zone is considered to be the one at the black dotted line in Figure 5. According to the short time scale and high gradient along the sliding direction, an uncertainty definitely exist and variations may occur around this contact location. When considering a sliding velocity of 50m/min and a circular contact width of 1mm, the time required for the hot surface to completely pass through the whole contact zone is approximately 1.2ms. A variation along the material flow direction could occur but most probably not with an amplitude close to the contact width. If a variation of half the contact width is assumed, ahead or at the back of the contact, this would lead to a variation between 10°C (over 140°C) at 500W and 50°C (over 550°C) at 2000W. This results in a potential variation between 7 and maximum 10% compared to the targeted temperature, which seems reasonably acceptable considering the complexity of the system.

The validation of the simulated results is not straight forward as measuring temperature in a sliding contact is still a real issue. Thermocouples could be embedded in one of the sliding bodies, which is highly

complex here considering the size of the samples and the sliding open configuration. Using an infrared camera would definitely provide additional data such as the temperature distribution but assessing the actual temperature is again challenging as it requires the perfect knowledge of the emissivity, which may vary locally depending on the surface conditions such as roughness or oxidation [28, 29]. Therefore, it is to date difficult to validate the simulated temperature fields via an experimental approach. One option to develop in a future work would be to implement two-color pyrometers that would provide local temperature measurements and avoiding issues related to the emissivity of the materials.

Nevertheless, for a validation purpose, the FE results were compared with the ones provided by an analytical model presented in [30]. When considering temperature fields below the melting point, the error between the temperatures computed via the two models remained below 10% which was considered to validate the numerical approach.

Finally, one can highlight that this analysis is valid for the given material pair. Simulated temperatures will indeed be affected if, for example, a more refractory alloy is employed such as a titanium or nickel based-alloy. Thermophysical properties will have to be accordingly updated and it is expected that the temperature profiles, especially along the depth, will differ due to a modified heat diffusion."

4. Experimental implementation

4.1. Upgraded experimental set-up

Based on the previous analyses, a specific mounting system was designed to fit the laser heating unit into the tribometer. A Laserline OTS5 optics was selected and combined with a 3kW diode laser, both from Laserline GmbH, via an optical fiber of 600μm with a numerical aperture of 0.2. The focal distance of 150mm resulted in a circular spot size of 1.2mm under a normal incidence on the surface. The final setup can be seen in Figure 10a with the different components and under operating conditions in Figure 10b. As discussed in Section 2.1, the mounting system resulted in a 57° incidence angle and an effective laser spot of 1.2 x 5.5mm on the counter surface.

The tribological experiments were carried out using a normalized AISI 1045 steel supplied as bars (80mm diameter x 500mm long) with hardness between 180 and 190 HB (yield stress 320 MPa; tensile strength - 696 MPa) and a ferritic-pearlitic microstructure.

Friction pins with a spherical diameter of Ø9mm were made of tungsten carbide with around 8% of cobalt binder and were TiN coated. Besides the fact that it is typically employed on cutting tools, this substrate material was intentionally selected as it is characterized by a high stiffness, high hardness and thus a good wear resistance. The PVD TiN coating was applied to reduce the material transfer phenomena and focus the study on the counterpart analysis without affecting the results by a potential catastrophic wear of the

pin. To eliminate the potential influence of surface roughness, friction pins were ground and polished down to Ra 0.3μm.

The apparent friction coefficient μ_{app} was provided by the ratio between the tangential F_t and the normal F_n forces in Eq. 5.

$$\mu_{app} = \frac{F_t}{F_n} \tag{5}$$

The term 'apparent friction coefficient' or 'macroscopic friction coefficient' is used since it differs significantly from the 'local friction coefficient' induced by adhesion at the pin-work material interface. The work conducted by Bowden and Tabor [31] proposes a simple decomposition in two contributions (Eq. 6):

$$\mu_{app} = \mu_{adh} + \mu_{plast} \tag{6}$$

Where, μ_{app} is the apparent friction coefficient, μ_{adh} the adhesive part and μ_{plast} is the contribution of the plastic deformation in the softest material (ploughing).

Only the apparent friction coefficient μ_{app} was considered in this study. Extracting both the adhesive and plastic would have been possible but would have required an intense post-processing either based on an analytical model as described by Claudin et al. [17] or a numerical procedure as developed by BenAbdelali et al. [18].

A constant normal load of 1200N was applied on the pin while the sliding velocity varied from 5 to 160m/min. The amplitude of the normal load was here selected to ensure the formation of a full plastic contact. If the Hertzian contact pressure does not make sense in that case, increasing the normal load once the onset of plastic yield is reached, intends to be sure that the contact is fully plastic and that the contact area is large enough to become insensitive to any remaining surface defects or variations in terms of topography. The average plastic contact pressure can be estimated to be 3 times the yield stress of the material [32], so around 1.5 GPa in the present configuration.

Several laser power amplitudes from 1000 to 3000W were applied, without running all the possible combinations. Each of these tests lasted minimum 5 seconds and was replicated in order to estimate the uncertainty. The values presented in the following sections are the average of the signal recorded during the experiments over a steady state period whereas the error bars represent $\pm$ the standard deviation.

4.2. Friction coefficient

The Figure 11a shows the evolution of the apparent friction coefficient versus time when activating the laser at 1000W and 3000W. Over the first 0.5s, friction was stable with an average value close to 0.18. While it remained stable over the whole test without pre-heating, it suddenly increased to 0.4 when activating the

laser pre-heating system at 1000W and exceeded 0.6 at 3000W. Interestingly, the apparent friction coefficient dropped back to the initial value of 0.18 when deactivating the counter surface pre-heating.

An average value of μ_{app} was then extracted over the laser activation period and a stable sliding distance, resulting in the bar chart presented in Figure 11b. It can be observed that friction increased as soon as pre-heating was applied for each tested sliding velocity. However, when increasing the latter, the increase in μ_{app} appeared to be lower with values close to 0.3 at 80 and 160m/min when applying 2000W against 0.4 at 5m/min with 1000W. This could be directly connected to the lower temperatures achieved when increasing the velocity, even with a higher laser power (Fig. 6).

It is important to emphasize that the power mentioned in this experimental section concerns the setting of the laser source. It does not obviously corresponds to the actual input power on the counter surface as this highly depends on the surface absorption coefficient. Peng [33] reported an absorptivity close to 0.6-0.7, leading to a maximum possible power input of around 2000W, in agreement with the simulations performed in Section 3.1.

4.3. Surface topography

The surface topography of the contact tracks was analyzed with an Alicona G5 focus-variation microscope to assess any changes in the contact morphology (Fig. 12).

The scratched surface was found to become smoother as the laser power increased. Some abrasive grooves and micro-ploughing marks were still observed at 1000W (Fig. 12a-b) while the contact zone appeared highly smooth at 3000W (Fig. 12c-d). However, a larger contact area could also be reported with, for example, an increase by 50% when applying 1000W compared to a non-heated test, and a factor larger than 2 when increasing the laser power from 1000W to 3000W. This could explain the increase recorded on the apparent friction coefficient.

Interestingly, the indentation depth was relatively constant and around 20μm but whereas a material side flow was observed at 1000W (Fig. 12a-b), a specific topography could be noted at 3000W as shown in Figures 12c-d. The primary profile (Fig. 12d) is characterized by a 140μm high peak (M_1) and a gap region (M_2) which could correspond to the formation of a keyhole typically found in laser welding [34]. These two observations tend to show that melting occurred ahead of the contact zone and that the pin was sliding on a thin partially melted layer. The similar indentation depths highlight that the increase in the contact width was not due to a deeper penetration amplified by the softening of the counter surface but by a more complex phenomena such as a side flow of the melted bath combined to a thermal expansion in the normal direction.

4.4. Near-surface evolution

In order to investigate the subsurface properties, samples were extracted in both sliding and transverse directions. Each was mounted, polished with SiC grinding papers up to 1200 followed by diamond based

suspensions down to 1μm and finally etched in 2 % Nital solution. Optical analyses were then performed using a ZEISS microscope.

The first analyses focused on the extreme specific case of the lowest sliding velocity of 5m/min. The Figure 13 shows that the microstructure of the AISI1045 steel was modified by the laser pre-heating and formed a white layer beneath the contact zone. The initial ferritic-pearlitic microstructure, that could still be seen in the bulk material, was completely dissolved and transformed into a new one difficult to characterize with an optical microscope. The width of this transformed region appeared to be larger than the contact area (Fig. 13a-c) and increased from 2.5 to 4.2mm when increasing the laser power from 1000W to 3000W. This can be correlated to the increase in terms of friction previously reported (Fig. 11) and a potential increase in the ploughing component of the apparent friction coefficient. To the same extent, higher the laser power, deeper the affected depth with approximately 200μm at 1000W versus 500μm when set at 3000W. These findings are in agreement with those presented in Figures 7 and 9 from which a phase transformation was expected at a so low speed, and an increasing depth with the increasing input power.

Microharness measurements were performed along the depth and at different transverse locations (Fig. 13b-d). It can be seen that the hardness close to the top surface increased up to 800HV whereas the bulk hardness was around 200HV. However, increasing the power to 3000W led this hardness to be reached over 400μm compared to only the first 20 to maximum 50μm at 1000W. These hardness profiles are characteristic of those obtained by laser quenching where a sudden increase in the hardness can be achieved, contrary to induction hardening where the transition is smoother [35]. This proves that a hard martensite phase could have been formed in this white layer, most probably not completely before the material entered the contact zone.

Zooming in on the near surface region (Fig. 14) highlighted the differences in terms of microstructure. At 1000W, grain boundaries are still visible with the cementite fully dissolved beyond the transition zone (Fig. 14a). At 3000W, a really fine microstructure was generated confirming the complete dissolution of the ferrite and pearlite (Fig. 14c). The mechanical action of the pin also affected the microstructure over 10 to 20μm from the near surface within the white layer as finer and elongated grains could be observed as shown in Figure 14a when applying 1000W. This was however not that obvious at 3000W and on the migrographs in the sliding direction (Fig. 14c-d). An assumption is that a post-dynamic transformation still occurred once the steel left the contact zone, once the mechanical loadings of the pin were released and cooling took place. This would definitely have to be confirmed by deeper and further analyses at a much lower scale.

Based on the simulation results and the map shown in Figure 9, the experiments run at 80m/min were also carefully analyzed as no phase transformation was supposed to occur. The cross sections in both slid-

ing and transverse directions (Fig. 15a-b) show that the ferritic-pearlitic microstructure was not affected when applying 2000W, confirming the prediction of the developed model. A small near surface layer with a thickness of approximately 5μm could still be identified in Figure 15a while the shear deformation along the sliding direction was visible as presented in Figure 15b.

The same analyses were conducted on the sample run without the laser preheating. The deformed microstructure could be observed in the sliding direction (Fig. 15d) as well as a deformed near surface layer in the transverse direction (Fig. 15c). However, the microstructure did not seem to be the same as the one generated with a laser power of 2000W and corresponded more to a work-hardened one. Additionally, the grain elongation in the sliding direction was more intense at 2000W than without preheating.

Based on these results, it was assumed that the thin layer identified in Figure 15a was the result of the severe plastic deformation combined to the heat generated both by friction and the preheating system which led to a grain refinement mechanism as reported in a previous work [36]. The increase in μ_{app} observed at this higher sliding velocity (Fig. 11) could thus be explained by a slight increase of the contact area but also by the formation of a thin more adhesive layer.

5. Conclusions

This paper focused on the development of a new laser-based heating system fitted on an open tribometer to perform high temperature friction and wear testing. It presented a combined numerical and experimental study to design the system, assess the achievable input temperatures in the contact and highlight the potential phase transformation depending on the sliding and preheating conditions. The important findings of this work are as follows:

- Maximum temperatures between 450°C and 600°C could be reached at the contact zone with sliding velocities up to 100m/min;
- Extreme thermal kinetics of 3 to 5.10^5 $°C/s$ could be achieved which are definitely of interest as far as high speed processes are concerned;
- When employed with steels, the austenitic transformation could be activated which shows that, besides the maximum targeted temperature, the occurrence of a phase transformation should be carefully considered;
- The apparent friction coefficient was found to increase as soon as a laser preheating was applied over the whole range of sliding velocities;

- Whereas no specific and severe material transfer was observed onto the friction pin, the detailed analysis of the contact track emphasized a relatively smooth sliding process dominated by abrasive and microploughing phenomena;

- Depending on the sliding and preheating conditions, contact could occur between the friction pin and a soft and fully transformed material, leading to whether a drastic increase in the contact area or the formation of a more adhesive thin surface layer;

- Finally, the developed numerical model provided relevant and consistent results compared to the experimental observations.

The last conclusion presents an interesting perspective as it could be used to deeply investigate the interaction with the preheated surface. Combined thermomechanically coupled simulations taking into account not only the laser source but also the friction pin itself could be developed and the final thermomechanical loadings withstood by the steel counter-surface could be extracted.

From the experimental point of view, the main limitation of the current system is the lack of local temperature measurements and the fact that only the laser power can be controlled. A further improvement of the system will be to implement a pyrometry based technique to assess the temperature right at the exit of the contact to increase the understanding of such specific tribological behavior.

Acknowledgments

This research was supported by the French National Research Agency within the framework of the ANR JCJC INSIDE project (ANR-17-CE8-0027-01).

References

[1] J. Archard, The temperature of rubbing surfaces, Wear 2 (1959) 438–455.

[2] Z. Mane, J.-L. Loubet, C. Guerret, L. Guy, O. Sanseau, L. Odoni, L. Vanel, D. Long, P. Sotta, A new rotary tribometer to study the wear on reinforced rubber material, Wear 306 (2013) 149–160.

[3] B. Tran, K. Tieu, S. Wan, H. Zhu, Lubricant as a sticking-scale inhibitor on high temperature sliding contact, Tribology International 140 (2019).

[4] A. Ghiotti, F. Sgarabotto, S. Bruschi, A novel approach to wear testing in hot stamping of high strength boron steel sheets, Wear 302 (2013) 1319–1326.

[5] M. Rahman, J. Ding, A. Beheshti, X. Zhang, A. Polycarpou, Elevated temperature tribology of ni alloys under helium environment for nuclear reactor applications, Tribology International 123 (2018) 372–384.

[6] J. Hardell, S. Hernandez, S. Mozgovoy, L. Pelcastre, C. Courbon, B. Prakash, Effect of oxide layers and near surface transformations on friction and wear during tool steel and boron steel interaction at high temperatures, Wear 330-331 (2015) 223 – 229. 20th International Conference on Wear of Materials.

[7] M. Hoić, M. Hrgetić, J. Deur, Design of a pin-on-disc-type cnc tribometer including an automotive dry clutch application, Mechatronics 40 (2016) 220–232.

[8] A. Tavasci, F. Arizzi, D. Dini, E. Rizzi, Heat flux evaluation in high temperature ring-on-ring contacts, Wear 330–331 (2015) 320–326.

[9] C. Courbon, M. Fallqvist, J. Hardell, R. MSaoubi, B. Prakash, Adhesion tendency of pvd tialn coatings at elevated temperatures during reciprocating sliding against carbon steel, Wear 330–331 (2015) 209–222.

[10] I. Velkavrh, M. Lüchinger, K. Kern, S. Klien, F. Ausserer, J. Voyer, A. Diem, M. Shreiner, W. Tillmann, Using a standard pin-on-disc tribometer to analyse friction in a metal forming process, Tribology International 114 (2017) 418–428.

[11] C. Mary, S. Fouvry, J. Martin, B. Bonnet, Pressure and temperature effects on fretting wear damage of a cu-ni-in plasma coating versus ti17 titanium alloy contact, Wear 272 (2011) 18–37.

[12] R. Gautam, U. Rao, R. Tyagi, High temperature tribological properties of ni-based self-lubricating coatings deposited by atmospheric plasma spray, Surface & coatings technology 372 (2019) 390–398.

[13] Y. Meng, J. Xu, Z. Jin, B. Prakash, Y. Hu, A review of recent advances in tribology, Friction 8 (2020) 221–300.

[14] M. Olsson, B. Stridh, S. Söderberg, U. Jansson, Sliding wear of hard materials - the importance of a fresh countermaterial surface, Wear 124 (1988) 195–216.

[15] L. Sterle, F. Pusavec, M. Kalin, Determination of friction coefficient in cutting processes: comparison between open and closed tribometers, Procedia CIRP 82 (2019) 101–106.

[16] M. Olsson, S. Söderberg, S. Jacobson, S. Hogmark, Simulation of cutting tool wear by a modified pin-on-disc test, International Journal of Machine Tools and Manufacture 29 (1989) 377 – 390.

[17] C. Claudin, A. Mondelin, J. Rech, G. Fromentin, Influence of a straight oil on friction at the tool-workmaterial interface in machining, International Journal of Machine Tools and Manufacture 50 (2010) 681–688.

[18] H. BenAbdelali, C. Courbon, J. Rech, W. BenSalem, A. Dogui, P. Kapsa, Identification of a friction model at the tool-chip-workpiece interface in dry machining of a aisi 1045 steel with a tin coated carbide tool, Journal of Tribology 133 (2011) 042201.

[19] Cora, K. Namiki, M. Koç, Wear performance assessment of alternative stamping die materials utilizing a novel test system, Wear 267 (2009) 1123–1129.

[20] M. Fallqvist, M. Olsson, The influence of surface defects on the mechanical and tribological properties of vn-based arc-evaporated coatings, Wear 297 (2013) 1111 – 1119.

[21] A. Yanagida, T. Kurihara, A. Azushima, Development of tribo-simulator for hot stamping, Journal of Materials Processing Technology 210 (2010) 456–460.

[22] C. Boher, S. L. Roux, L. Penazzi, C. Dessain, Experimental investigation of the tribological behavior and wear mechanisms of tool steel grades in hot stamping of a high-strength boron steel, Wear 294–295 (2012) 286–295.

[23] S. Mozgovoy, J. Hardell, L. Deng, M. Oldenburg, B. Prakash, Tribological Behavior of Tool Steel Under Press Hardening Conditions Using Simulative Tests, Journal of Tribology 140 (2017). 011606.

[24] S. P. F. C. Jaspers, J. H. Dautzenberg, Material behaviour in conditions similar to metal cutting: flow stress in the primary shear zone, Journal of Materials Processing Technology 122 (2002) 322 – 330.

[25] T. Miokovic, V. Schulze, O. Vöhringer, D. Löhe, Prediction of phase transformations during laser surface hardening of aisi 4140 including the effects of inhomogeneous austenite formation, Materials Science and Engineering A 435–436 (2006) 547–555.

[26] T. Miokovic, J. Schwarzer, V. Schulze, O. Vöhringer, D. Löhe, Description of short time phase transformations during the heating of steels based on high-rate experimental data, Journal de Physique IV 120 (2004) 591–598.

[27] M. Avrami, Kinetics of phase change – i general theory, Journal of Chemical Physics 7 (1939).

[28] M. Doubenskaia, M. Pavlov, S. Grigoriev, I. Smurov, Definition of brightness temperature and restoration of true temperature in laser cladding using infrared camera, Surface and Coatings Technology 220 (2013) 244–247. Proceedings of the fifth workshop RIPT (Les Rencontres Internationales sur la Projection Thermique).

[29] M. Ignatiev, L. Okorokov, I. Smurov, V. Martino, G. Bertolon, G. Flamant, Laser assisted machining : process control based on real-time surface temperature measurements, Journal de Physique IV Proceedings 04 (1994) C4–65–C4–68.

[30] N. Rykalin, A. Uglov, I. Zuev, A. Kokora, Laser and electron beam materials processing, 1988.

[31] F. P. Bowden, D. Tabor, The Friction and Lubrication of Solids, Oxford University Press, 1951.

[32] K. Johnson, Contact Mechanics, Cambridge University Press, 1987.

[33] Q. Peng, An analytical solution for a transcient temperature field during laser heating a finite slab, Applied Mathematical Modeling 40 (2016) 4129–4135.

[34] J. Svenungsson, I. Choquet, A. Kaplan, Laser welding process – a review of keyhole welding modelling, Physics Procedia 78 (2015) 182 – 191. 15th Nordic Laser Materials Processing Conference, Nolamp 15.

[35] P. D. Babu, G. Buvanashekaran, K. R. Balasubramanian, Experimental studies on the microstructure and hardness of laser transformation hardening of low alloy steel, Transactions of the Canadian Society for Mechanical Engineering 36 (2012) 241–258.

[36] G. Jacquet, G. Kermouche, C. Courbon, D. Tumbajoy, J. Rech, Effect of sliding velocity on friction-induced microstructural evolution in copper, IOP Conference Series - Materials Science and Engineering 63 (2014). 6th International Conference on Nanomaterials by Severe Plastic Deformation.

List of Tables

A	Yield strength (MPa)
B	Hardening modulus (MPa)
C	Strain rate sensitivity coefficient (viscosity)
C_{Avr}	Velocity constant (s^{-1})
F_n	Normal Force (N)
F_t	Tangential forces (N)
$f_{A,i}$	Percentage of austenite formed at t_i (%)
k	Boltzmann constant ($eV.K^{-1}$)
m	Thermal softening coefficient
n	Hardening coefficient
n_{Avr}	Avrami constant
T	Temperature of the workpiece (°C)
T_0	Room temperature (°C)
T_f	Melting temperature of the work material (°C)
ΔH	Activation enthalpy (ferrite to austenite) (eV)
$\dot{\varepsilon}_0$	Reference plastic strain rate (s^{-1})
$\dot{\varepsilon}_p$	Plastic strain rate (s^{-1})
μ_{adh}	Adhesive part of the apparent friction coefficient
μ_{app}	Apparent friction coefficient
μ_{plast}	Contribution of the plastic deformation in the softest material (ploughing)

Table 1 — Nomenclature

Steel	A [MPa]	B [MPa]	n	C	$\dot{\varepsilon_0}$ [/s]	m	T_m [$^\circ C$]	T_0 [$^\circ C$]
AISI 1045	553.1	600.8	0.234	0.0134	1	1	1460	25

Table 2 — Johnson-Cook model parameters for AISI 1045 ([24])

	Temperature (°C)	AISI1045
Specific Heat $(J.Kg^{-1}.K^{-1})$	0	420
	100	470
	200	521
	300	571
	400	622
	500	672
	600	722
	700	733
	800	823
	900	874
Conductivity $(J.m^{-1}.s^{-1}.K^{-1})$	100	50.7
	400	41.9
	700	30.1
	1000	26.8
Density (Kg/m^3)	14450	7850
E (GPa)	630	207
ν	0.3	0.3

Table 3 — Thermal properties of AISI1045 steel.

Parameter	Symbol	Value
Percentage of formed austenite at t_i	$f_{A,i}$	[%]
Temperature	T	[°K]
Boltzmann constant	k	$8.617 \times 10^{-5} eV.K^{-1}$
Avrami constant	n	1.585
Velocity constant	C	$2.84 \times 10^{20} s^{-1}$
Activation enthalpy (ferrite to austenite)	ΔH	$4.185 eV$

Table 4 — Parameters of the model from Miokovic et al. [25, 26] to compute the percentage of formed austenite.

List of Figures

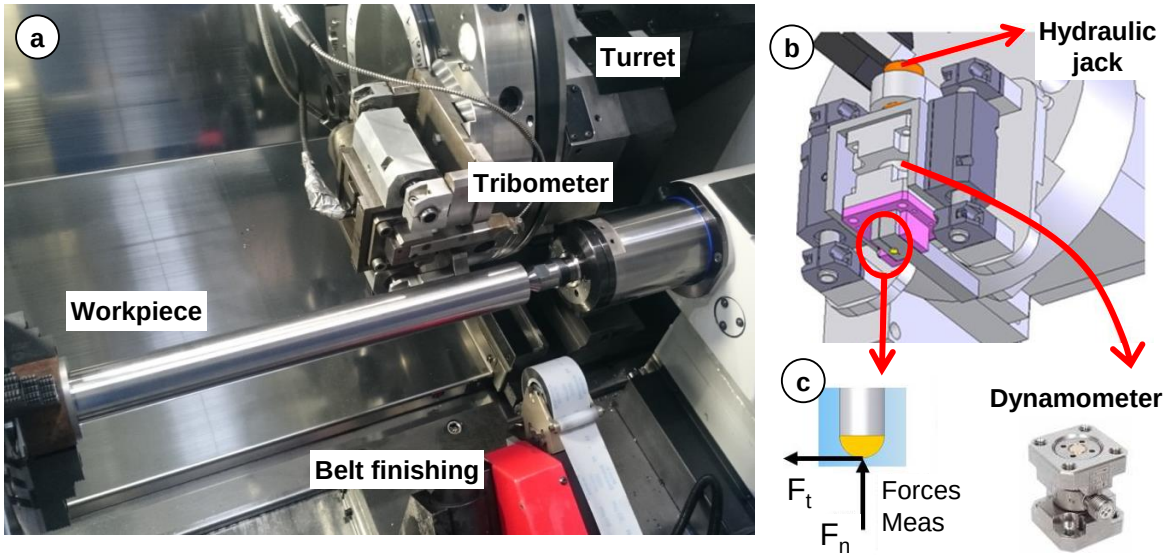

Fig. 1 — (a) Overview of the initial configuration of the tribological setup; b) close view of the tribometer and c) instrumentation.

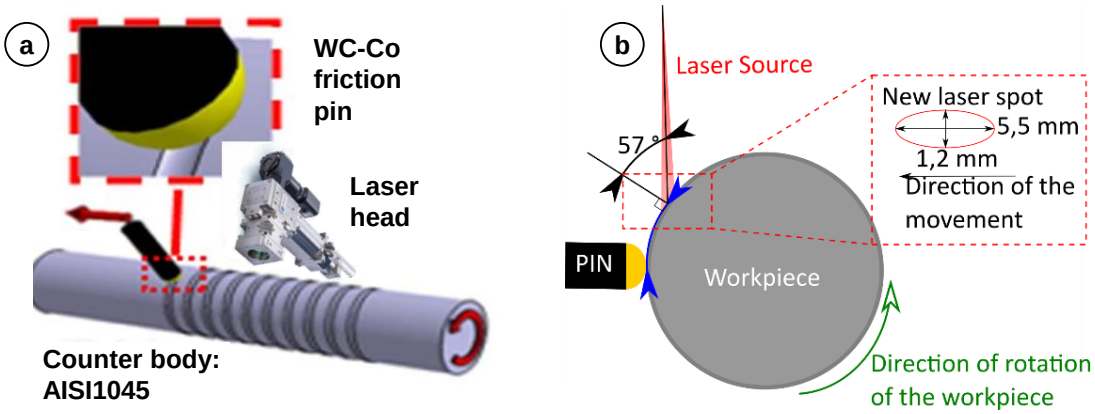

Fig. 2 — (a) Principle of the friction test and b) schematic of the laser pre-heating system with the laser head illustrated in a).

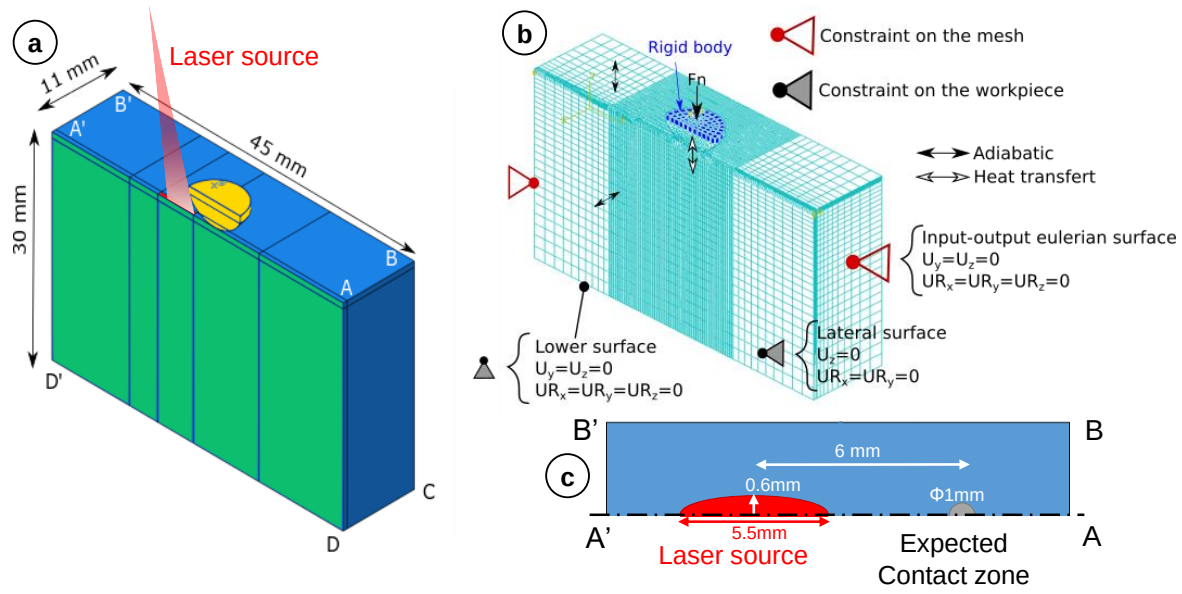

Fig. 3 — (a) Geometry of the 3D ALE model; b) mesh and boundary conditions; c) top view with the schematic of the laser spot and expected contact area.

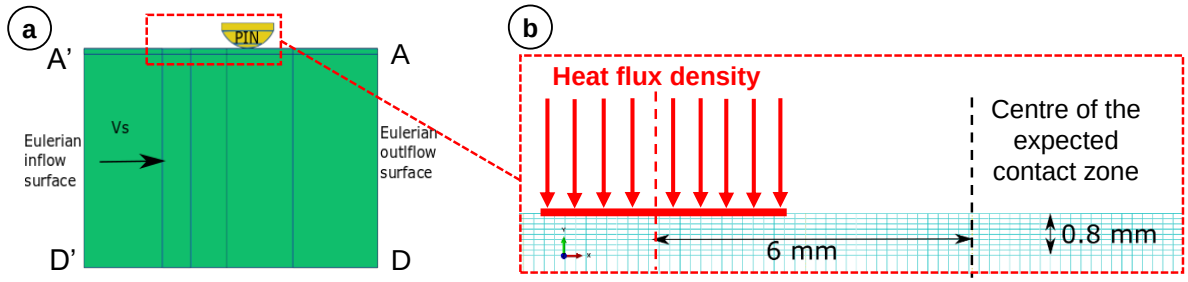

Fig. 4 — (a) Side view of the model with the region of interest and b) with the laser beam being model as a heat input and meshed workpiece.

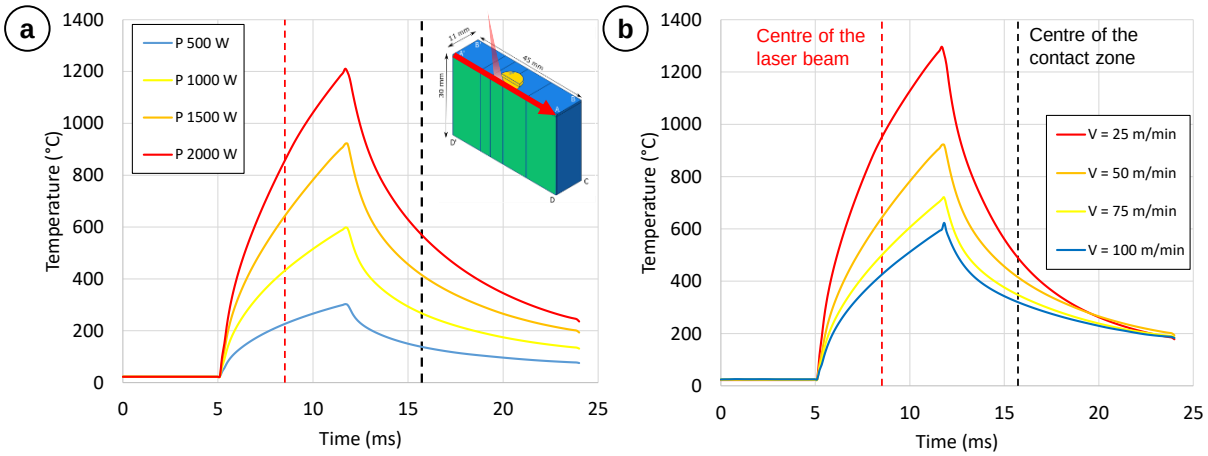

Fig. 5 — Temperature profiles at the top surface a) at a constant velocity of 50m/min when varying the power input and b) at a constant power input of 1500W and a varying sliding velocity – the red dotted line represents the axis of the laser spot, the black one being the center of the contact zone.

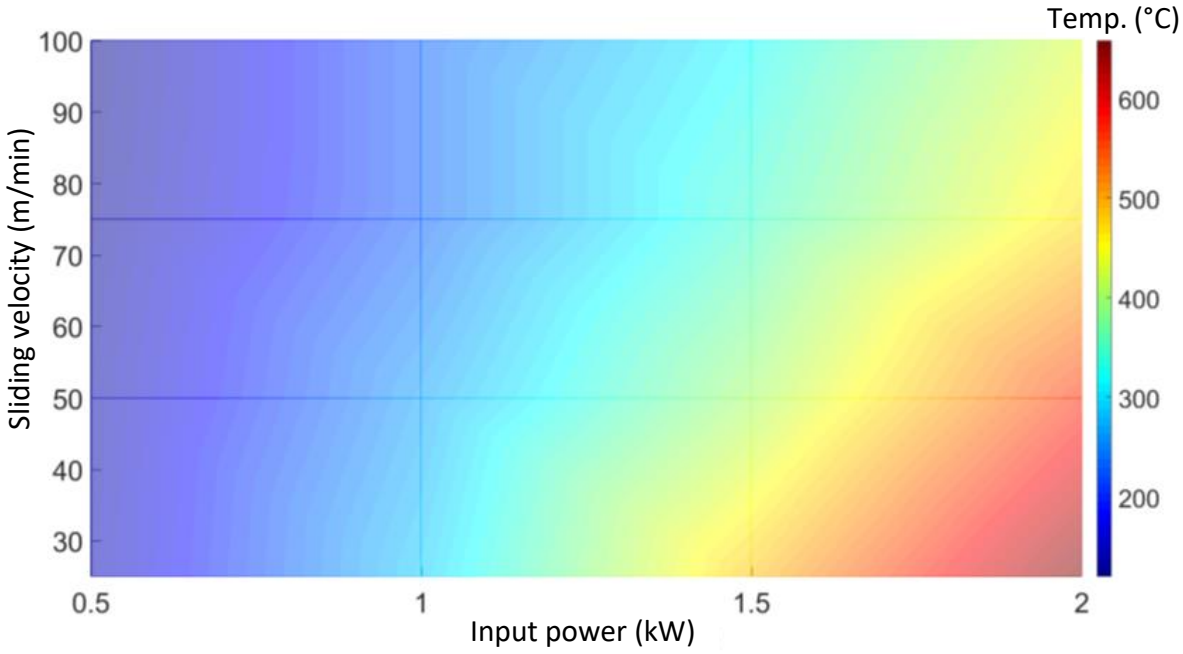

Fig. 6 — Mapping of the temperature at the contact zone depending on the input power and sliding velocity.

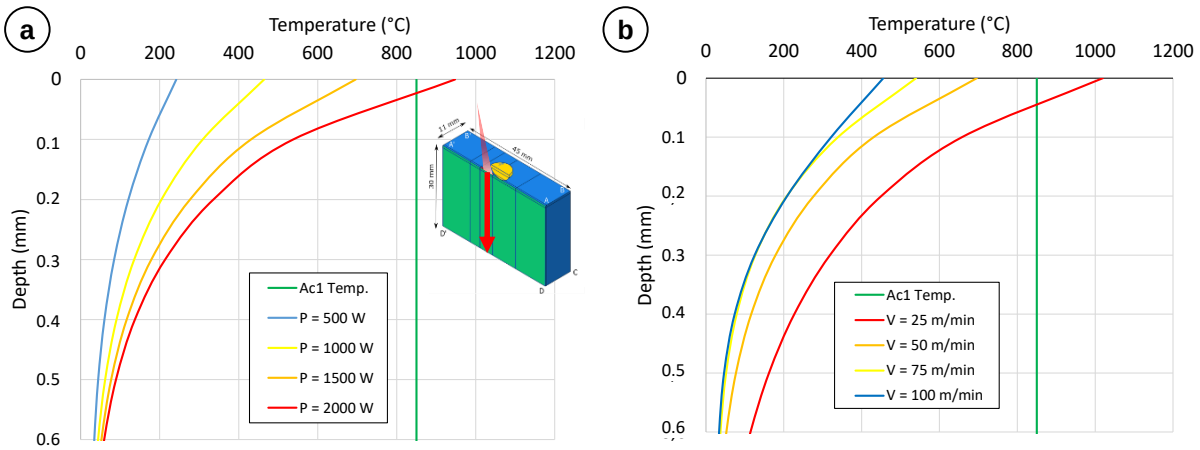

Fig. 7 — Temperature profiles along the depth below the center of the laser spot a) at a constant velocity of 50m/min when varying the power input and b) at a constant power input of 1500 W and a varying sliding velocity.

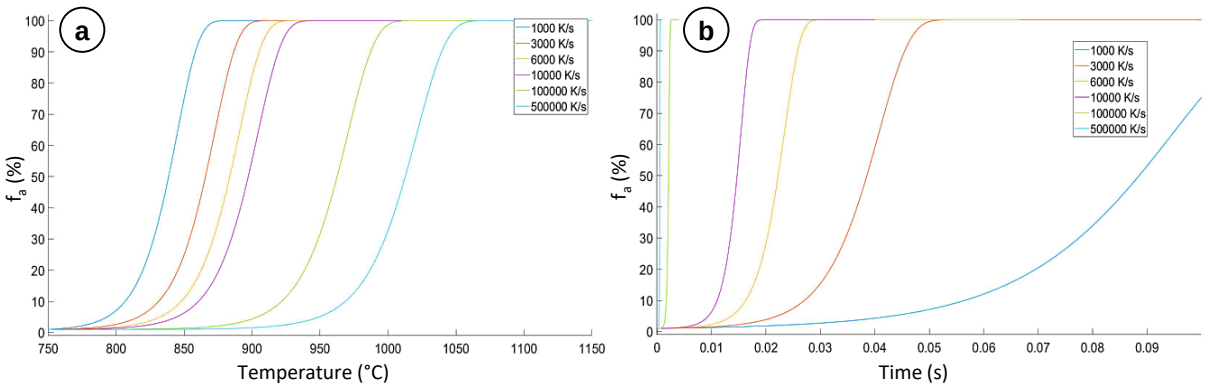

Fig. 8 — Percentage of formed austenite depending a) on the temperature and b) on the time after the beginning of the transformation for different heating rates.

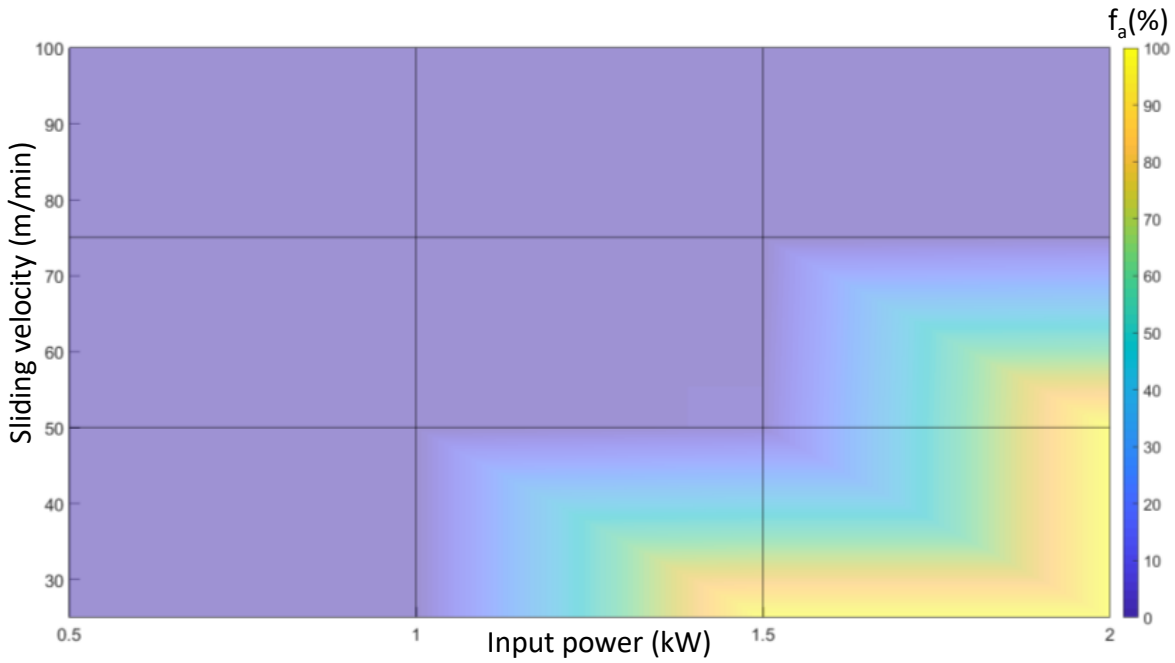

Fig. 9 — Mapping of the fraction of formed austenite below the heated region depending on the input power and sliding velocity.

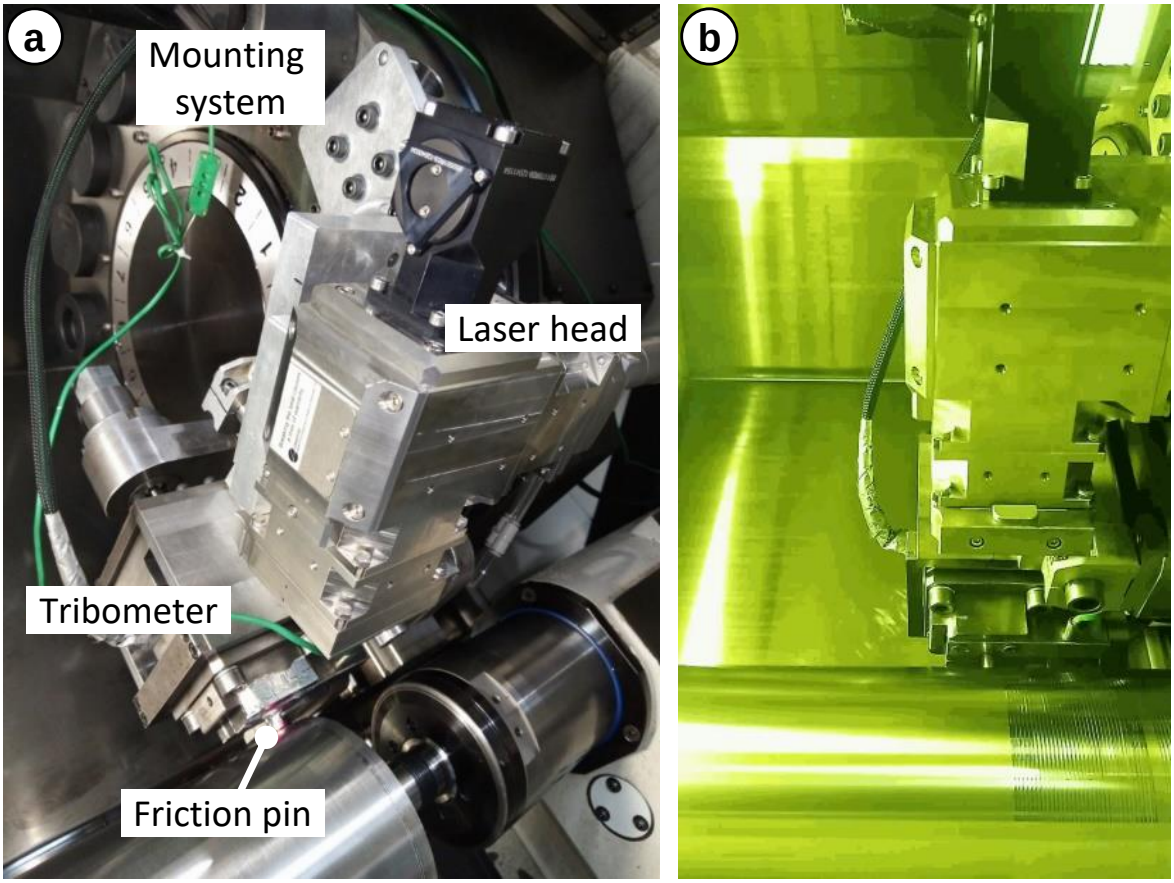

Fig. 10 — Implementation of the laser heating system into the upgraded tribometer: a) overview of the laser head and b) side view of the operating system and formation of the contact track.

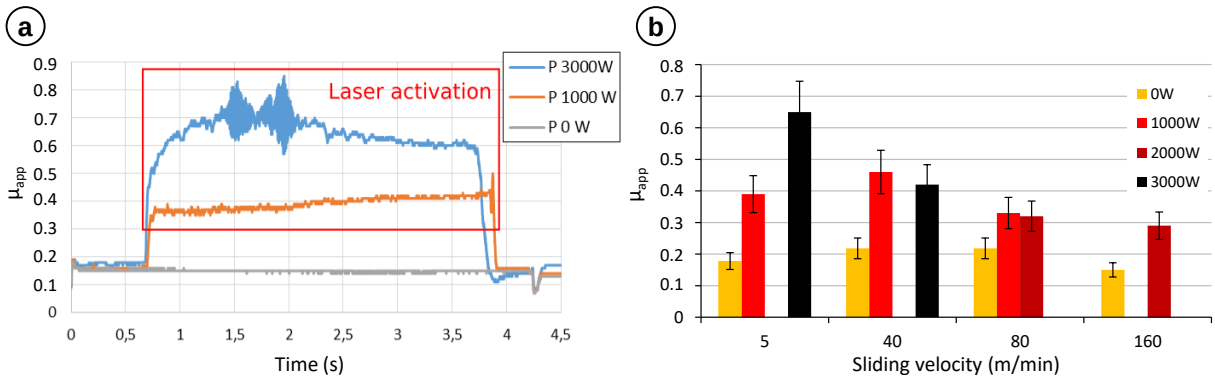

Fig. 11 — Evolution of the apparent friction coefficient: a) versus time at 5m/min and b) versus the sliding velocities with different laser power inputs.

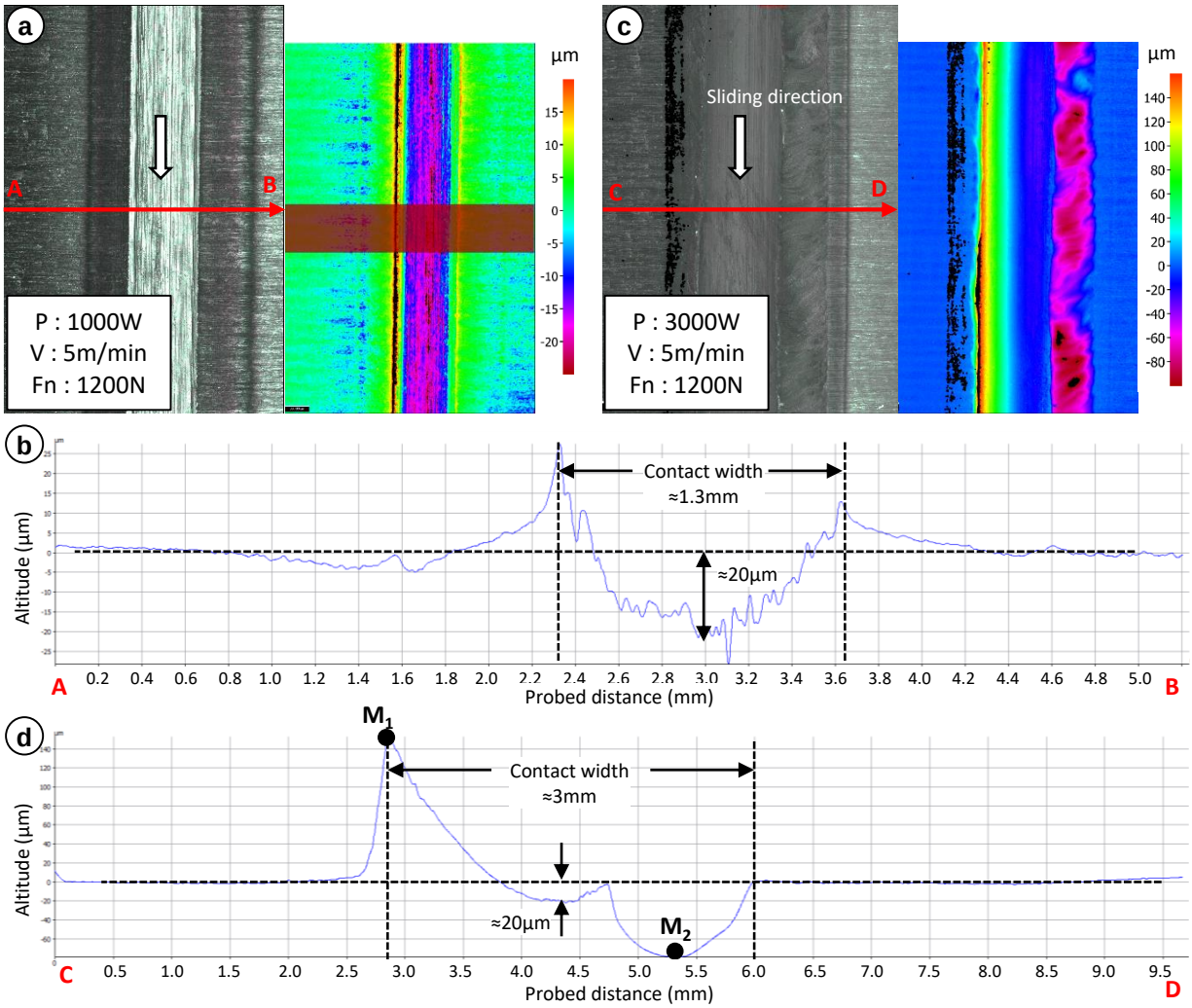

Fig. 12 — Examples of contact track topography extracted at 5m/min with a laser power of a) 1000W with the corresponding primary profile along the A-B line (b); b) with a laser power of 3000W with the corresponding primary profile along the C-D line (d).

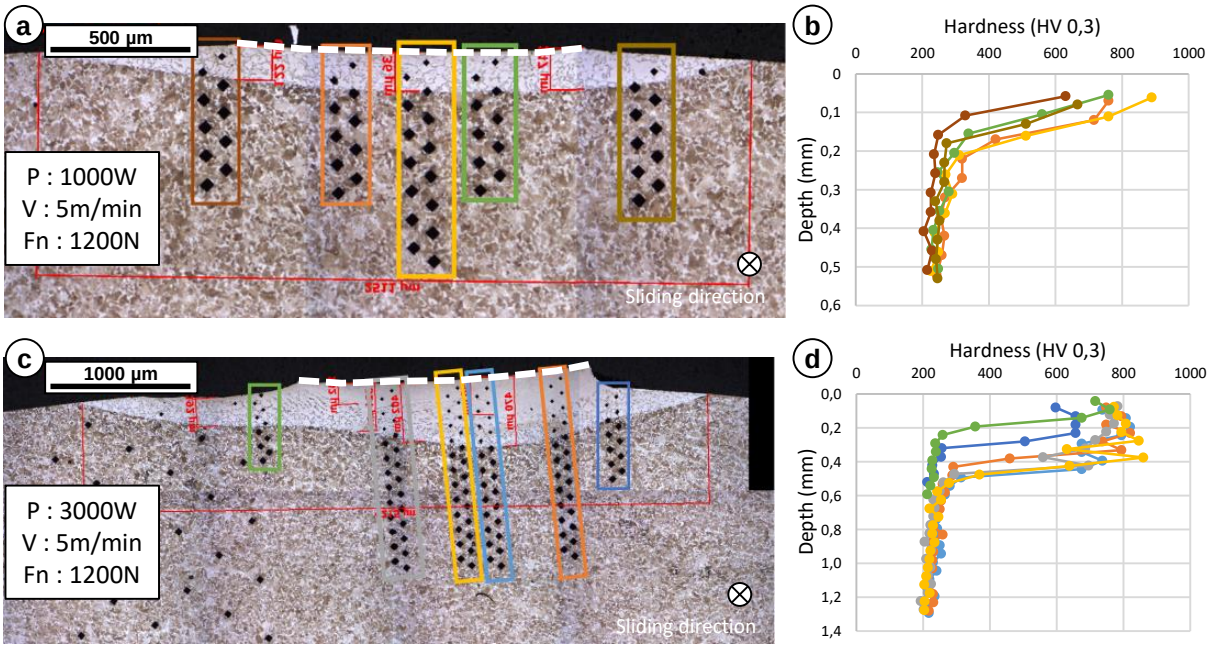

Fig. 13 — Overview of the microstructure beneath the contact zone in the transverse direction at 5m/min when applying a) a laser power of 1000W or b) 3000W with the corresponding hardness profiles (b,d) – the white dotted line being the actual contact width.

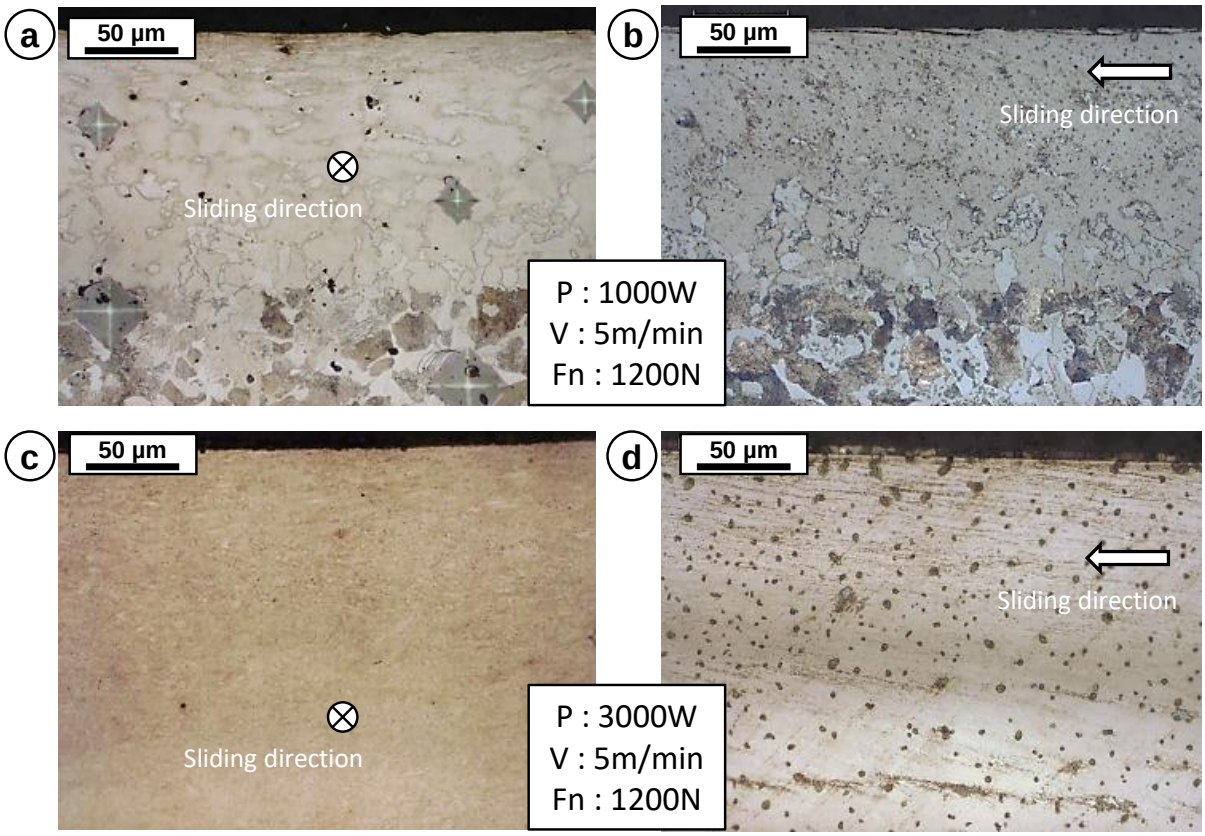

Fig. 14 — Near surface microstuctures at 5m/min when applying a laser power of 1000W (a,b) or 3000W (c,d) both in the transverse (a,c) and sliding direction (b,d) directions.

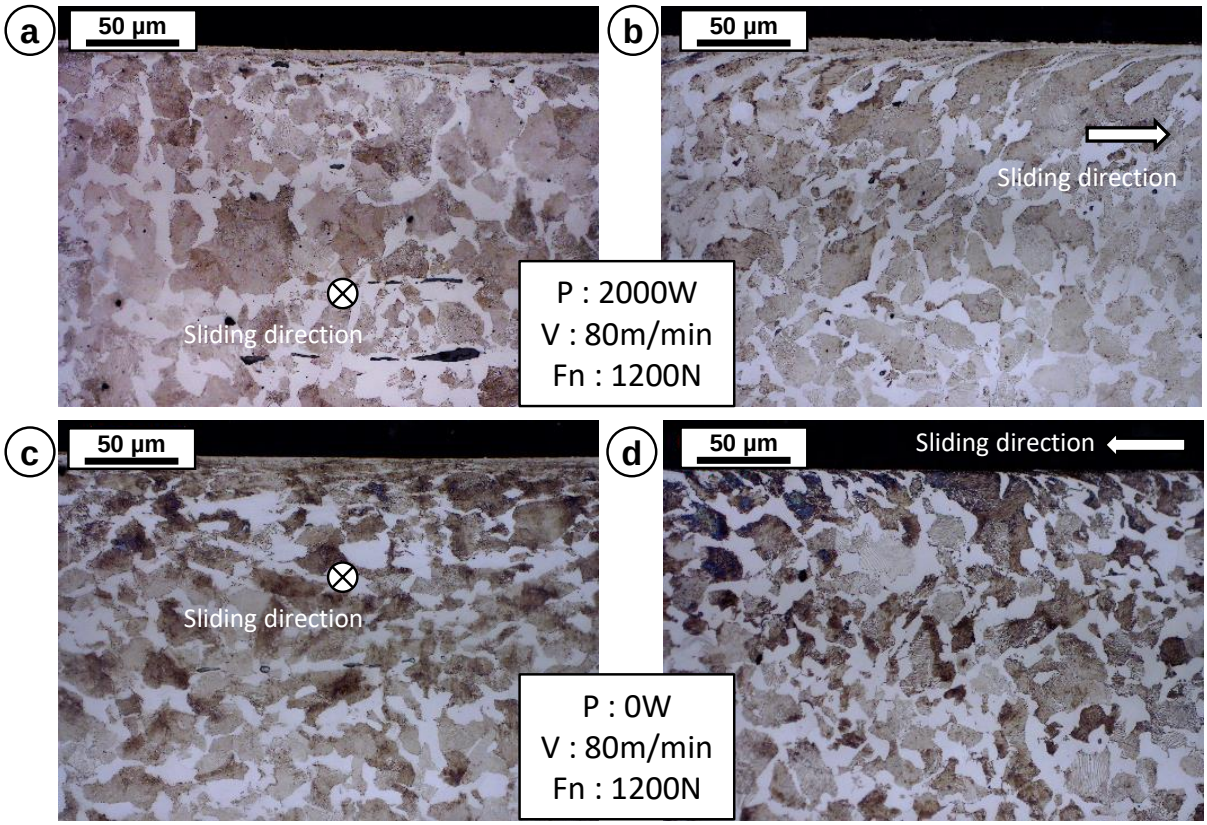

Fig. 15 — Near surface microstuctures at 80m/min when applying a laser power of 2000W (a,b) or without a laser preheating (c,d) both in the transverse (a,c) and sliding direction (b,d) directions.